Applied Catalysis B: Environmental 307 (2022) 121163

Contents lists available at ScienceDirect

Applied Catalysis B: Environmental

journal homepage: www.elsevier.com/locate/apcatb

Heterogenizing homogeneous cocatalysts by well-designed hollow MOF-based nanoreactors for efficient and size-selective CO_2 fixation

Ze Qin [a], Hao Li [a], Xianfeng Yang [b], Liyu Chen [a], Yingwei Li [a,*], Kui Shen [a,*]

[a] Key Laboratory of Fuel Cell Technology of Guangdong Province, School of Chemistry and Chemical Engineering, South China University of Technology, Guangzhou 510640, China
[b] Analytical and Testing Centre, South China University of Technology, Guangzhou 510640, China

ARTICLE INFO

Keywords:
CO_2 fixation
Heterogeneous catalysts
Heterogenization
Hollow nanoreactors
Metal-organic frameworks

ABSTRACT

The fixation of CO_2 with epoxides is a promising strategy to reduce CO_2 emission. However, homogeneous halogen-based cocatalysts are often requisite for most heterogeneous catalysts to obtain desired activities, which significantly complicates the subsequent product purification/separation. Herein, we report the heterogenization of homogeneous Br-based cocatalysts by encapsulating them into stable and recyclable ZIF-8-based hollow nanoreactors (ZIF-8-HS) for efficient CO_2 fixation. The synthesis involves in epitaxial growth of a size-controlled ZIF-8 layer on hollow ZIF-67 spheres prepared by using Br-contained surfactants as templates, followed by etching the unstable ZIF-67 shell. In ZIF-8-HS, the Br-contained surfactants can serve as efficient cocatalysts to activate substrates, while the microporous ZIF-8 shell possesses abundant intrinsic active sites and offers the cocatalysts a confined homogeneous environment. Impressively, ZIF-8-HS shows high activity, good size-selectivity and excellent recyclability for the CO_2 fixation with epoxides, fully exploiting the respective advantages of homogeneous CTAB and heterogeneous ZIF-8 for this reaction.

1. Introduction

The excessive emission of CO_2 from the combustion of fossil fuels has been considered as a primary factor for global warming and ocean acidification [1]. Therefore, in recent decades, a variety of methodologies have been developed to tackle the enormous emissions of CO_2 and implement the carbon neutralization [2–5], among which the transformation of CO_2 into diverse valuable products has attracted considerable attention, since CO_2 is an abundant, cheap, nontoxic and inexhaustible C1 feedstock despite its undesirable impact on environment [6,7]. In particular, the chemical fixation of CO_2 with epoxides has been widely deemed as an efficient approach to close the carbon cycle due to its 100% atomic economy and the resultant valuable cyclic carbonate products, which are extensively applied as aprotic polar solvents, fuel additives, electrolytes and organic synthetic intermediates in chemical industry [8–11]. The major bottleneck, however, lies in the activation of inert CO_2 molecules with high thermodynamic stability, which is urgent to be overcome by developing efficient catalytic systems.

Owing to the advantages of easy separation and good reusability as well as devisable molecule confinement effect, heterogeneous catalysts are much more attractive and glorious in chemical industry as compared with their homogenous counterparts [12–18]. In respect of the fixation of CO_2 with epoxides, a large number of heterogeneous catalysts have been developed in the last decade, mainly including zeolites [19,20], supported metal nanoparticles [21,22], porous organic polymers (POPs) [23,24], and especially metal-organic frameworks (MOFs) [25,26], an important subclass of porous materials constructed from tunable metal ions/clusters and organic ligands. Unfortunately, for most heterogeneous catalysts, the desired catalytic performances for CO_2 fixation can only be achieved in the presence of a homogeneous halogen-based cocatalyst to activate epoxides, which greatly complicates the subsequent product separation and purification processes [27–30]. Moreover, the repetitive addition of homogeneous cocatalysts in each cycle can also raise operation complexity, frustrating the industrialization of these catalyst systems. Practicably, the integration of homogeneous catalysts into various porous hosts (such as covalent graft [31], in-situ polymerization [32] and efficient encapsulation of homogeneous catalysts in the nanopores of hosts [33]) provides a feasible strategy to tackle these problems. Nevertheless, the pore blocking with diffusion limitation, low stability toward leaching and unavoidable coverage of active sites by encapsulated cocatalysts can undoubtedly decrease the whole catalytic

* Corresponding authors.
E-mail addresses: liyw@scut.edu.cn (Y. Li), cekshen@scut.edu.cn (K. Shen).

https://doi.org/10.1016/j.apcatb.2022.121163
Received 13 December 2021; Received in revised form 25 January 2022; Accepted 29 January 2022
Available online 7 February 2022
0926-3373/© 2022 Elsevier B.V. All rights reserved.

performances of the resultant composites [31–33]. Given that MOFs have the advantages of good structural flexibility, tailorable functionality, high surface area and especially tunable pore size [34–36], we envision that the encapsulation of halogen-based cocatalysts into a unique hollow MOF structure with uniform continuous shell and high permselective properties may provide a more efficient way to heterogenize homogeneous cocatalysts for chemical fixation of CO_2.

Accordingly, herein, we report the fabrication of a new type of ZIF-8-based hollow nanoreactors (ZIF-8 is a highly stable MOF assembled by Zn ions and 2-methylimidazole ligands) encapsulating homogeneous alkyltrimethylammonium bromide (denoted as ZIF-8-HS) as highly active and reusable catalysts for the chemical fixation of CO_2 with epoxides. In our study, ZIF-8 is chosen as a host material because of its high stability, mild preparation condition, abundant uniformly-distributed Lewis acidic sites and well-defined micropores with small six-membered-ring windows of 0.34 nm [37–43], and hexadecyltrimethylammonium bromide (CTAB) is employed as a primary cocatalyst due to its good synergistic effects with many previously-reported heterogeneous catalysts on the chemical fixation of CO_2 [21,44]. Indeed, our control experiments also prove that the addition of homogeneous CTAB as a cocatalyst, which itself only show very poor catalytic activity, can boost above six times the catalytic activity of ZIF-8 for the fixation of CO_2 with epichlorohydrin (from 11% to 77%) (Fig. 1a). Furthermore, though ZIF-67 (ZIF-67 has the same sodalite topology as ZIF-8 but with Co ions as metal nodes) can also afford a high activity in the first run, its much lower stability and thus poorer recyclability as compared with ZIF-8 give a critical strike to its practical application, as revealed by its dramatically reduced epichlorohydrin conversions from 82% to 17%

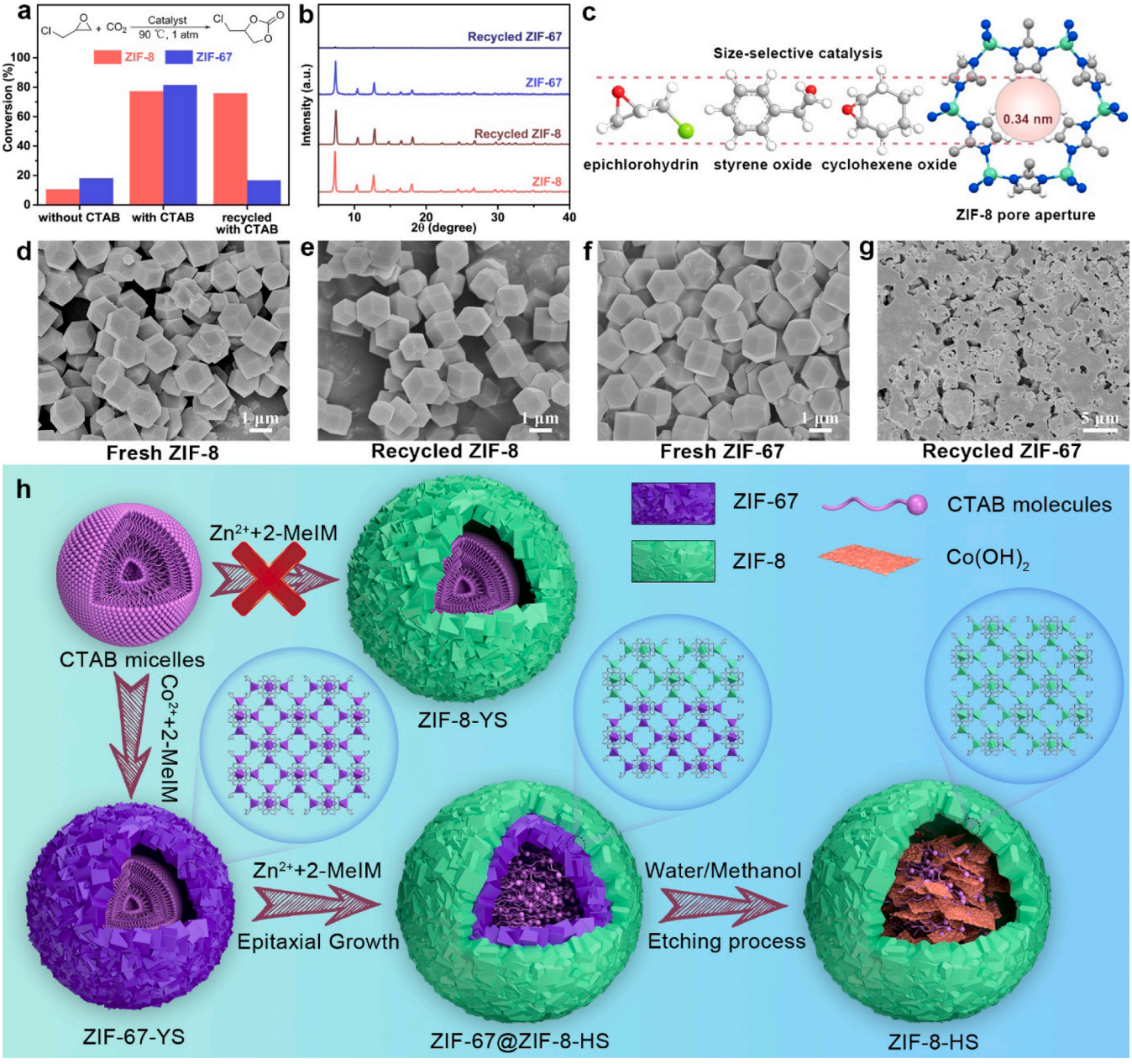

Fig. 1. (a) Conversions of epichlorohydrin for CO_2 fixation reaction over fresh or recycled ZIF-8 and ZIF-67 with or without CTAB as a cocatalyst (reaction conditions: 5.0 mmol of epichlorohydrin, 1 mol% of catalyst based on Zn or Co, 0.25 mol% of CTAB if need be, 1 atm of CO_2, 90 °C and 24 h; the epichlorohydrin conversions for recycled ZIF-8 and ZIF-67 were obtained in the third run). (b) PXRD patterns of fresh or recycled ZIF-8 and ZIF-67. (c) Concept of the size-selective cycloaddition between CO_2 and different epoxides with various sizes by using ZIF-8 as a catalyst. (d-g) SEM images of fresh ZIF-8 (d), recycled ZIF-8 (e), fresh ZIF-67 (f), and recycled ZIF-67 (g). (h) Schematic illustration of the preparation of the ZIF-8-HS nanoreactors.

after three runs (Fig. 1b, d-g and Fig. S1, S2). Inspired by these results and also previous advances in this field [11,45], we rationally design and prepare ZIF-8-HS with the idea that the encapsulated CTAB in the hollow nanoreactors can serve as an efficient co-catalyst to activate epoxides, while the stable and continuous ZIF-8 shell can not only provide abundant Lewis acidic sites with high intrinsic catalytic activity, but also offer CTAB an confined but permselective homogeneous environment to prevent its leaching (Fig. 1c and Fig. S3) [46], the combination of which is expected to bring about the high activity, good size-selectivity and excellent recyclability of ZIF-8-HS for the fixation of CO_2 with epoxides.

2. Experimental

2.1. Chemicals

All chemicals with analytical grade are purchased from commercial suppliers and used without any further treatment. Hexadecyltrimethylammonium bromide (CTAB, 99%, Aladdin), myristyltrimethylammonium bromide (TTAB, 99%, Aladdin), dodecyltrimethylammonium bromide (DTAB, 99%, Aladdin), cobalt(II) nitrate hexahydrate ($Co(NO_3)_2$•6 H_2O, 99%, Aladdin), 2-methylimidazole (2-MeIM, 98%, Aladdin), cobalt(II) chloride hexahydrate ($CoCl_2$•6 H_2O, AR, Aladdin), zinc(II) nitrate hexahydrate ($Zn(NO_3)_2$•6 H_2O, 99%, Guangzhou Donzhenghuabo), zinc(II) acetate dihydrate ($Zn(CH_3COO)_2$•2 H_2O, 99%, Aladdin), epichlorohydrin (AR, Aladdin), polyvinylpyrrolidone (PVP, MW 58000, Aladdin), epibromohydrin (98%, Macklin), glycidol (98%, Macklin), styrene oxide (98%, Macklin), cyclohexene oxide (98%, Macklin).

2.2. Materials preparation

2.2.1. Synthesis of ZIF-67-YS

In a typical synthesis, 1.079 g of CTAB (2.963 mmol) was completely dissolved in 250 mL of deionized water by ultrasonic treatment for 2 min and magnetic stirring for 30 min. Then, 1.35 mL aqueous solution of $Co(NO_3)_2$ (0.5 M) was injected to the above solution, which was further stirred for 30 min. Subsequently, 30 mL of aqueous solution containing 2.428 g of 2-MeIM (29.574 mmol) was added into the above pale pink solution. The reaction solution was left to stir for 4 h, and the obtained purple product was collected by centrifugation, washed with methanol and finally redispersed into methanol by ultrasonic treatment (the total volume is 50 mL) for further use.

2.2.2. Synthesis of ZIF-67 @ZIF-8-HS

In a typical synthesis, 157.6 mg of 2-MeIM was added into the above methanol solution containing ZIF-67-YS. Subsequently, another 50 mL of methanol solution containing $Zn(NO_3)_2$ (9.6 mM) was added into above solution under stirring. The mixed solution was further stirred for 12 h at room temperature. Finally, the resulting product was collected by centrifugation and washed with methanol.

2.2.3. Synthesis of ZIF-8-HS

The above as-prepared ZIF-67 @ZIF-8-HS was redispersed into 200 mL of mixed solution of methanol and deionized water (v: v = 1: 1) by ultrasound treatment, and then let it stand for about 3 h to selectively etch the unstable inner ZIF-67 layer in ZIF-67 @ZIF-8-HS. The obtained product (namely ZIF-8-HS) was harvested by centrifugation, washed with methanol and finally dried overnight at 60 °C for further use.

In addition, we have also attempted to directly prepare ZIF-8-HS by replacing $Co(NO_3)_2$.6 H_2O with $Zn(NO_3)_2$.6 H_2O in the first step, while keeping other conditions unchanged. However, no product was obtained possibly due to the poor crystallization activity between Zn ions and 2-methylimidazole molecules in a CTAB-contained aqueous solution.

2.2.4. Synthesis of m-ZIF-8-HS

The m-ZIF-8-HS with various shell thicknesses were synthesized by regulating the concentration of 2-MeIM and $Zn(NO_3)_2$ with other conditions being the same as ZIF-8-HS:

15.4 mM of 2-MeIM and 3.8 mM of $Zn(NO_3)_2$ for 0.4-ZIF-67 @ZIF-8-HS;
26.9 mM of 2-MeIM and 6.7 mM of $Zn(NO_3)_2$ for 0.7-ZIF-67 @ZIF-8-HS;
57.6 mM of 2-MeIM and 14.4 mM of $Zn(NO_3)_2$ for 1.5-ZIF-67 @ZIF-8-HS;
76.8 mM of 2-MeIM and 19.2 mM of $Zn(NO_3)_2$ for 2.0-ZIF-67 @ZIF-8-HS.

2.2.5. Synthesis of ZIF-8-HS-C_n

ZIF-8-HS-C_{12} and ZIF-8-HS-C_{14} were synthesized by using the same method as ZIF-8-HS except that the CTAB was displaced by DTAB and TTAB, respectively.

2.2.6. Synthesis of conventional ZIF-8

In a typical synthesis, 0.219 g of $Zn(CH_3COO)_2$•2 H_2O (1 mmol) was dissolved in 15 mL of deionized water, while 2.463 g of 2-MeIM (30 mmol) was dissolved in another 15 mL of deionized water. The two solutions were mixed under stirring and the resulting solution was transferred to a teflon reactor inside a stainless-steel autoclave. For hydrothermal synthesis, the above reactor was heated at 120 ºC for 24 h in a programmable oven under static condition, and then cooled down to room temperature. The obtained product was washed with methanol, collected by centrifugation, and finally dried overnight at 60 °C for further use.

2.2.7. Synthesis of conventional ZIF-67

In a typical synthesis, 0.476 g of $CoCl_2$•6H_2O (2 mmol), 0.600 g of PVP and 2.463 g of 2-MeIM (30 mmol) were mixed in 80 mL of methanol under stirring. Then the mixture was left undisturbed at room temperature for 12 h. The product was washed with methanol, collected by centrifugation, finally dried overnight at 60 °C for further use.

2.3. Characterizations

Powder X-ray diffraction patterns were collected by D8-Advance Bruker with Cu Kα radiation (40 kV, 40 mA, λ = 1.5406 Å). The BET surface areas and pore size measurements were gained from N_2 adsorption/desorption isotherms at 77 K using a Micromeritics ASAP 2020 M instrument. Before the analysis, the samples were degassed at 150 °C for 12 h. The morphology and elemental distributions of samples were determined using a transmission electron microscopy (TEM, JEOL, JEM-2100 F) with an EDX analysis system (Bruker Xflash 5030 T) at 200 kV. The surface morphology of samples was characterized by a high-resolution field-emission scanning electron microscopy (FESEM, HITACHI SU8220). The metal contents of samples were determined by atomic absorption spectroscopy (AAS, HITACHI Z-2300) and the CTAB content was measured by Ion chromatography (IC, Metrohm eco). The CO_2 and NH_3 temperature programmed desorption (CO_2-TPD and NH_3-TPD) measurements were obtained using a Micromeritics AutoChem II 2920 instrument. The sample was pre-heated at 300 °C for 1 h to clean the surface of the sample from moisture and other adsorbed gas. After that, the sample was cooled down to 50 °C and then equilibrated in a CO_2 or NH_3 flow for 1 h, followed by flushing in Ar for 1 h to remove any physisorbed molecules. The CO_2-TPD experiment was operated at 50–270 °C with a heating rate of 10 °C min^{-1} and holding at 270 °C for 2 h. The NH_3-TPD experiment was operated at 50–330 °C with a heating rate of 10 °C min^{-1}.

2.4. Catalytic test for cycloaddition reaction of epoxide and CO_2

In a typical procedure, 0.05 mmol of catalyst (based on Zn for ZIF-8-HS, Zn + Co for ZIF-67 @ZIF-8-HS, and Co for ZIF-67-YS) and 5.0 mmol of epoxide were introduced into a 10 mL Schlenk tube. Then the tube was vacuumed and purged with CO_2 by a balloon (1 atm). Then the reaction mixture was stirred for 24 h at 90 ℃ in an oil bath. After the reaction, the catalyst was recycled by centrifugation, washed with methanol and dried for next run. The supernatant was analyzed by GC-MS (Agilent, 7890B GC/5977 A MS) equipped with a DB-35 MS UI capillary column (0.25 mm × 30 m) to determine the conversion and selectivity.

3. Results and discussion

3.1. Synthesis and Characterization of ZIF-8-HS

The preparation procedure of the ZIF-8-HS is illustrated in Fig. 1 g. Briefly, the hollow ZIF-67 spheres with encapsulated CTAB micelles as yolks (denoted as ZIF-67-YS) were first synthesized by using CTAB as a representative soft template, which were then redispersed in a methanol solution containing Zn ions and 2-methylimidazole to epitaxially grow a ZIF-8 layer on the surface of hollow ZIF-67 spheres on account of their isostructural topology nature [47]. In this process, the demicellization of Co- and CTAB-containing yolks took place because of its greatly increased critical micelle concentration (CMC) [48–50], producing hollow ZIF-67 @ZIF-8 spheres with CTAB molecules highly dispersing in the interior cavities (denoted as ZIF-67 @ZIF-8-HS). Finally, ZIF-8-HS was obtained by treating the as-prepared ZIF-67 @ZIF-8-HS in a mixed water/methanol solution to etch the unstable inner ZIF-67 layer (Fig. S4). It is worth noting that we also attempted to directly prepare ZIF-8-HS by replacing $Co(NO_3)_2.6\ H_2O$ with $Zn(NO_3)_2.6\ H_2O$ in the first step, while keeping other conditions unchanged. However, no product was obtained possibly due to the poor crystallization activity between Zn ions and 2-methylimidazole molecules in a CTAB-contained aqueous solution (Fig. S5).

The changes of morphology, structure and composition from ZIF-67-YS to ZIF-67 @ZIF-8-HS and finally to ZIF-8-HS were investigated by field-emission scanning electron microscopy (SEM), transmission electron microscopy (TEM) and high-angle annular dark-field scanning TEM (HAADF-STEM). As shown in Fig. 2a1-a6 and S6, ZIF-67-YS has a particle size of about 920 nm, and the crack-free shell consists of intergrown polycrystals of ZIF-67 nanocubes with a thickness of about 160 nm. The corresponding energy dispersive X-ray spectroscopy (EDS) elemental mapping analysis (Fig. 2a7) confirms the uniformly distributed Co, N, C elements in the shell, abundant Br element in both of the interior cavity and shell, and highly enriched Co element in the Co- and CTAB-containing yolk formed at nucleation stage. After epitaxial growth, the obvious change in surface morphology from nanocube to truncated rhombic dodecahedron and the increase of particle size from about 920 nm to about 1080 nm, as well as the generation of a zinc-based ZIF-8 layer are observed for ZIF-67 @ZIF-8-HS (Fig. 2b1-b7 and Fig. S7). In addition, the strong EDX signal of Br element within a spherical cavity with ~937 nm in diameter indicates no evident leaching of CTAB, because linear CTAB molecules is too large (0.43 × 2.35 nm) to penetrate the small windows (0.34 nm) of the thick ZIFs shell. Delightedly, the successful selective etching of the unstable inner ZIF-67 can be pithily revealed by SEM, TEM, STEM and EDS mapping images (Fig. 2c1-c7 and Fig. S8). The resultant ZIF-8-HS exhibits unvaried particle size and surface morphology, while the inner ZIF-67 layer of ZIF-67 @ZIF-8-HS is completely collapsed and transformed into cobalt hydroxide nanosheets [37,51], which is accompanied by the decreased shell thickness from about 230 nm for ZIF-67 @ZIF-8-HS to about 78 nm for ZIF-8-HS. The Zn element is still located in the shell and the Co element is distributed in the interior cavity due to the formation of cobalt hydroxide. More importantly, the uniformly distributed and strong EDX signal of Br element in the interior cavity indicates no crack in shell is formed after the etching process due to the much better stability of ZIF-8 than ZIF-67 under the etching condition. In addition, the similar distributions of Br and Co elements in the spherical cavity with nearly identical diameters (about 939 nm) in their EDS elemental mappings reveals that all of CTAB molecules have been successfully encapsulated in the cavity of ZIF-8-HS (Fig. S8).

Powder X-ray diffraction (PXRD) was used to investigate the crystal structures of various resultant samples. As shown in Fig. 2d, all the diffraction peaks of ZIF-67-YS, ZIF-67 @ZIF-8-HS and ZIF-8-HS match well with those of simulated ZIF-8, confirming their identical sodalite-type structures with good crystallinities. Then N_2 adsorption/desorption experiments were performed to investigate the pore characteristics and specific surface areas of various samples. As illustrated in Fig. 2e, both of ZIF-67-YS and ZIF-67 @ZIF-8-HS show Type I sorption isotherm behaviors and high N_2 uptakes at low pressure, which are corresponding to their intrinsic micropores of ZIF-8/ZIF-67. However, the sorption isotherm of the ZIF-8-HS is a combination of Type I and Type IV, suggesting the presence of both micropores (below 1.5 nm) and mesopores (10–80 nm) in its structure, which can be attributed to the preservation of stable microporous ZIF-8 shell and the formation of local voids after the selective etching of unstable ZIF-67 nanocrystals, respectively. The corresponding pore size distribution curves further confirm that all samples have the same intrinsic micropores of ZIF-8/ZIF-67 with an average pore size of about 0.6 nm (Fig. 2 f and Table S1). As expected, the BET surface area of the ZIF-67 @ZIF-8-HS is calculated to be 1351 m^2g^{-1}, which is much higher than that of ZIF-67-YS (816 m^2g^{-1}) due to the demicellization of Co- and CTAB-containing yolks. In addition, the BET surface area of ZIF-8-HS (1195 m^2g^{-1}) is also lower than that of ZIF-67 @ZIF-8-HS because of the presence of cobalt hydroxide nanosheets in its interior cavity. Furthermore, the contents of Zn and Co in various samples were measured by atomic absorption spectroscopy (AAS), while that of CTAB was detected by ion chromatography (IC). As shown in Fig. 2g, the CTAB content is decreased from 15.2 wt% for ZIF-67-YS to 12.6 wt% for ZIF-67 @ZIF-8-HS due to the presence of CTAB-free ZIF-8 species in the latter. Importantly, after etching the unstable ZIF-67 layer, the resultant ZIF-8-HS still shows a high CTAB content of 18.5 wt%, suggesting that the stable and continuous ZIF-8 shell can efficiently prevent CTAB from leaching. In addition, Co content also shows a similar tend as CTAB content because the ZIF-67 species in ZIF-67-YS has been finally transformed into cobalt hydroxide nanosheets, which are encapsulated in the cavity of ZIF-8-HS (Fig. S9). All these results confirm that the well-designed ZIF-8-HS nanoreactors are composed of a continuous microporous ZIF-8 hollow shell and abundant soluble CTAB molecules encapsulated in its interior cavity.

3.2. Synthesis and characterization of ZIF-8-HS-C_n and m-ZIF-8-HS

We can easily extend our strategy to the construction of ZIF-8-HS encapsulating other kinds of alkyltrimethylammonium bromides with different length of alkyl chain (denoted as ZIF-8-HS-C_n, where n represents the number of carbon atoms of alkyl chain) (Fig. 3a, b and Figs. S10-S14). As shown in Fig. 3a1 and b1, both of ZIF-8-HS-C_{12} and ZIF-8-HS-C_{14} exhibit a similar sphere morphology but reduced average particle sizes as compared with ZIF-8-HS. TEM, STEM and corresponding element mapping images confirm their hollow structures with a continuous ZIF-8 shell of around 58 nm and 51 nm for ZIF-8-HS-C_{12} and ZIF-8-HS-C_{14}, respectively, in the interior cavities of which high contents of Br element can be detected (Fig. 3a2-a5 and b2-b5). Interestingly, no desired hollow nanoreactors can be obtained when using n-octyltrimethylammonium bromide or decyltrimethylammonium bromide as a soft template (Fig. S15). Furthermore, to investigate the influence of shell thickness on the catalytic activity of nanoreactors, we also prepared a series of ZIF-8-HS with various shell thicknesses by controlling the concentrations of Zn^{2+} and 2-methylimidazole in the epitaxial growth process (denoted as m-ZIF-8-HS, where m stands for the

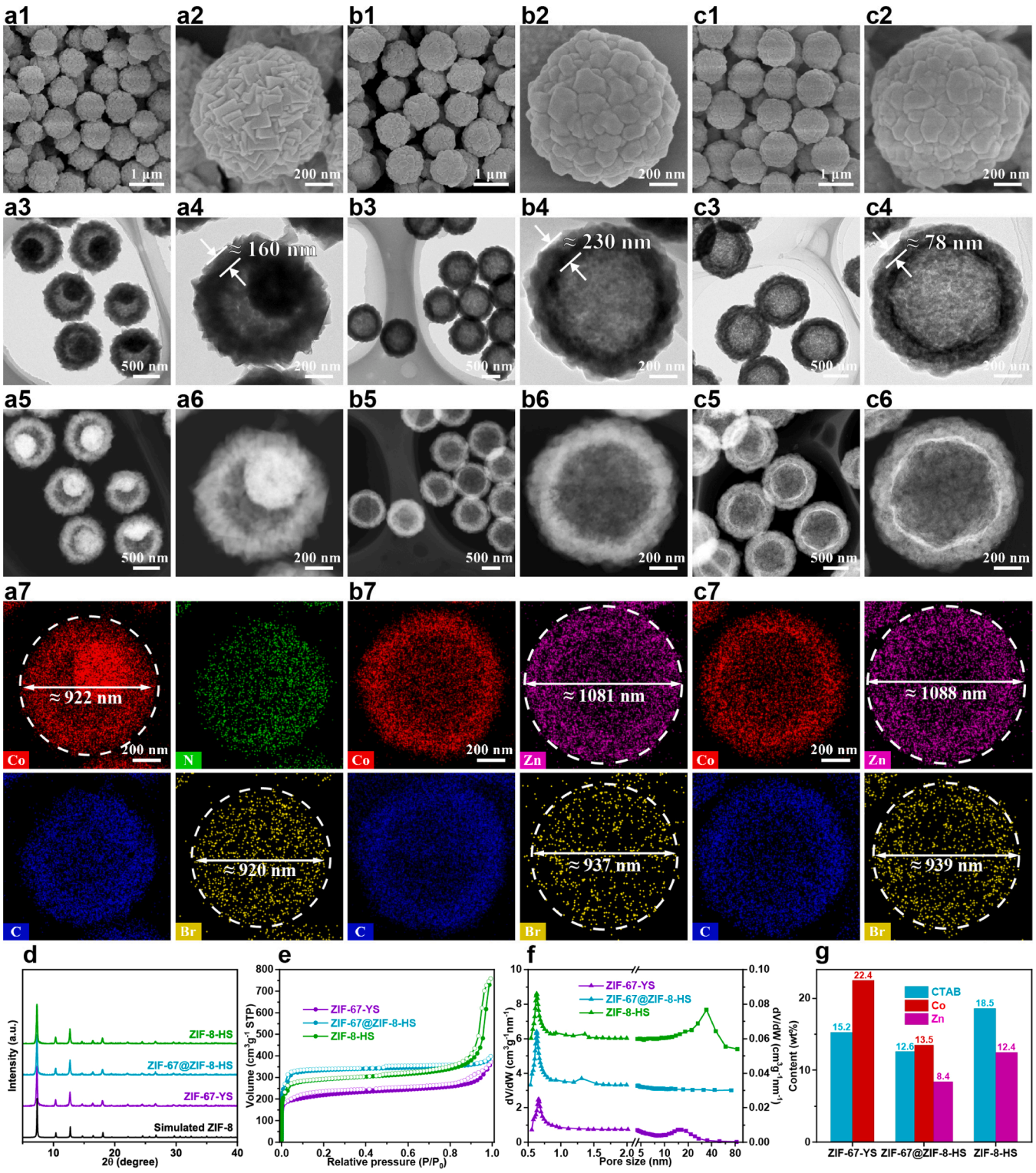

Fig. 2. (a1-c1, a2-c2) SEM, (a3-c3, a4-c4) TEM, (a5-c5, a6-c6) HAADF-STEM, and (a7-c7) EDS mapping images of ZIF-67-YS (a1-a7), ZIF-67 @ZIF-8-HS (b1-b7) and ZIF-8-HS (c1-c7). (d) PXRD patterns, (e) N_2 adsorption/desorption isotherms, (f) pore size distributions and (g) contents of representative element of various samples.

concentration ratio of 2-methylimidazole to that for preparing ZIF-8-HS, while keeping the molar ratio of $Zn(NO_3)_2.6\ H_2O$/2-methylimidazole unchanged). As expected, the shell thickness can be well adjusted from 43 nm for 0.4-ZIF-8-HS (Fig. 3c1-c4 and Fig. S16a) to 61 nm for 0.7-ZIF-8-HS (Fig. 3d1-d4 and Fig. S16b), and then to 104 nm for 1.5-ZIF-8-HS (Fig. 3e1-e4 and Fig. S16c), all of which have a similar sphere morphology and hollow structure to ZIF-8-HS. However, when further increasing the shell thickness to about 132 nm, the hollow structure of the corresponding 2.0-ZIF-8-HS is partly broken into small dispersive ZIF-8 crystals (Fig. 3f1-f4 and Fig. S16d). On the other hand, we have also attempted to further reduce the shell thickness by regulating the concentrations of 2-MeIM to 7.7 mM and $Zn(NO_3)_2$ to 1.9 mM. However, the resultant 0.2-ZIF-8-HS display a fragile morphology with many holes on their surface (Fig. S17). Based on the above observations, the

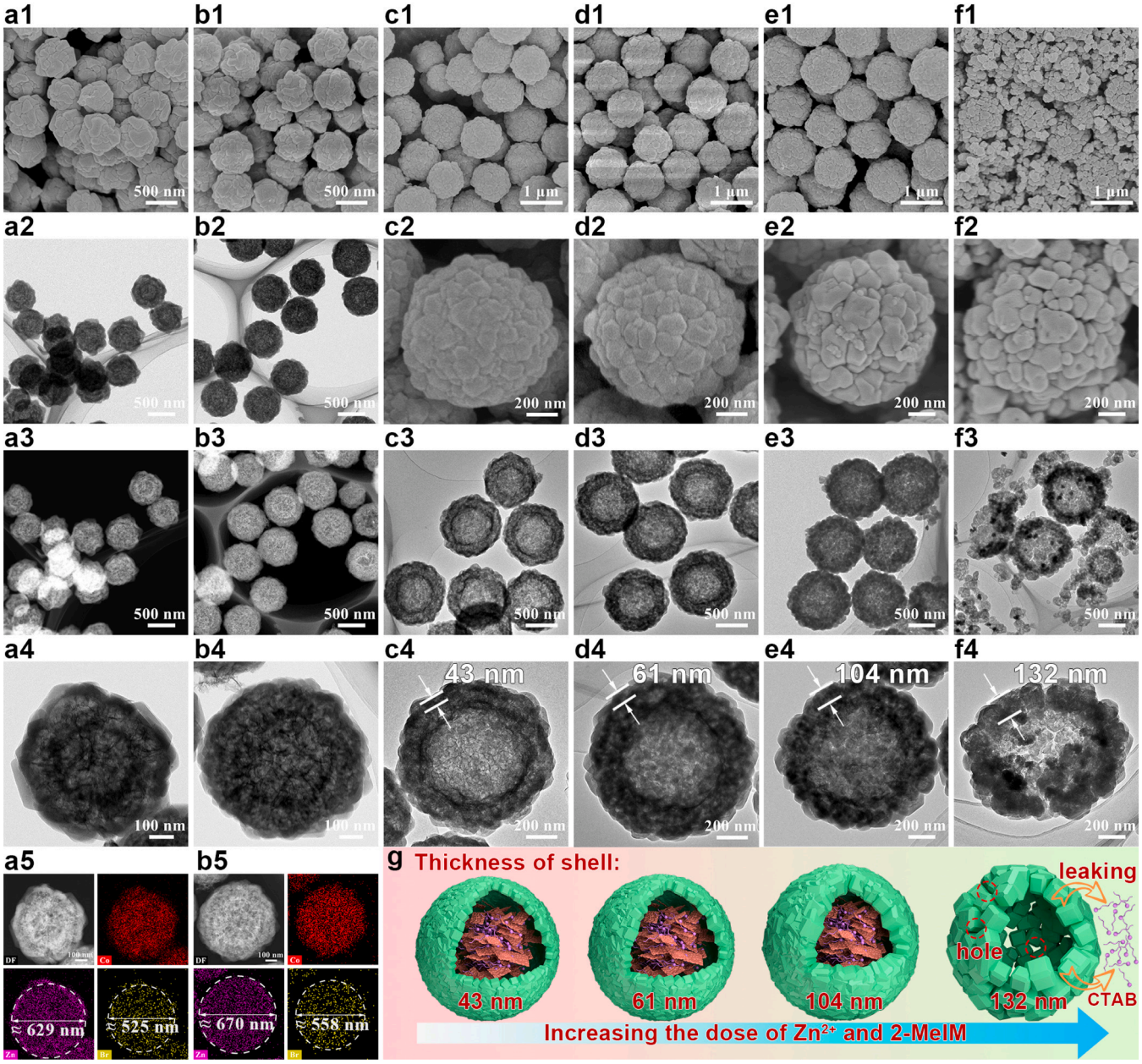

Fig. 3. (a1, b1) SEM, (a2, b2, a4, b4) TEM, (a3, b3, a5, b5) HAADF-STEM and EDS mapping images of ZIF-8-HS-C_{12} (a1-a5) and ZIF-8-HS-C_{14} (b1-b5). (c1-f1, c2-f2) SEM and (c3-f3, c4-f4) TEM images of 0.4-ZIF-8-HS (c1-c4), 0.7-ZIF-8-HS (d1-d4), 1.5-ZIF-8-HS (e1-e4) and 2.0-ZIF-8-HS (f1-f4). (g) Schematic illustration of the structural features of m-ZIF-8-HS with various shell thicknesses prepared by adjusting the concentrations of 2-methylimidazole and Zn^{2+}.

structural features of m-ZIF-8-HS with various shell thicknesses prepared by just adjusting the precursor concentration is described schematically in Fig. 3 g. It is obvious that we should control the shell thickness of m-ZIF-8-HS below 132 nm to obtain unbroken nanoreactors and thus prevent the leaching of CTAB molecules from their interior cavities.

3.3. Catalytic tests for the chemical fixation of CO_2

Subsequently, the chemical fixation of CO_2 with epichlorohydrin was carried out over various catalysts under 1 atm of CO_2 pressure. As shown in Fig. 4a, ZIF-67-YS is very catalytically active for this reaction, giving an epichlorohydrin conversion of 97% after 24 h, which is much higher than that of conventional ZIF-8 counterpart (11% after 24 h), indicating that the encapsulated CTAB in ZIF-67-YS can serve as an efficient cocatalyst for this reaction. After the epitaxial growth of a ZIF-8 layer on ZIF-67-YS, the resultant ZIF-67 @ZIF-8-HS shows a slightly lower catalytic activity with 82% conversion of epichlorohydrin after 24 h, since the new ZIF-8 layer would undoubtedly decelerate the mass diffusion of reactants. As expected, after etching the inner ZIF-67 layer of ZIF-67 @ZIF-8-HS, the obtained ZIF-8-HS exhibits the remarkably enhanced activity, giving a high conversion of 98% with above 99% selectivity of chloromethyl ethylene carbonate after 24 h. It is worth noting that both of cobalt hydroxide nanosheets and CTAB show very poor catalytic activities for this reaction, as revealed by their very low conversions under the same reaction conditions (Table S2, entries 1–3). Therefore, it is obvious that the high catalytic activity of ZIF-8-HS can be reasonably attributed to the synergistic effect between the continuous ZIF-8 shell with abundant Lewis acidic sites and the encapsulated CTAB as an efficient cocatalyst. Then various m-ZIF-8-HS catalysts were also tested for this reaction to investigate the influence of shell thickness on catalytic activity [52]. As shown in Fig. 4b, with the increase of shell

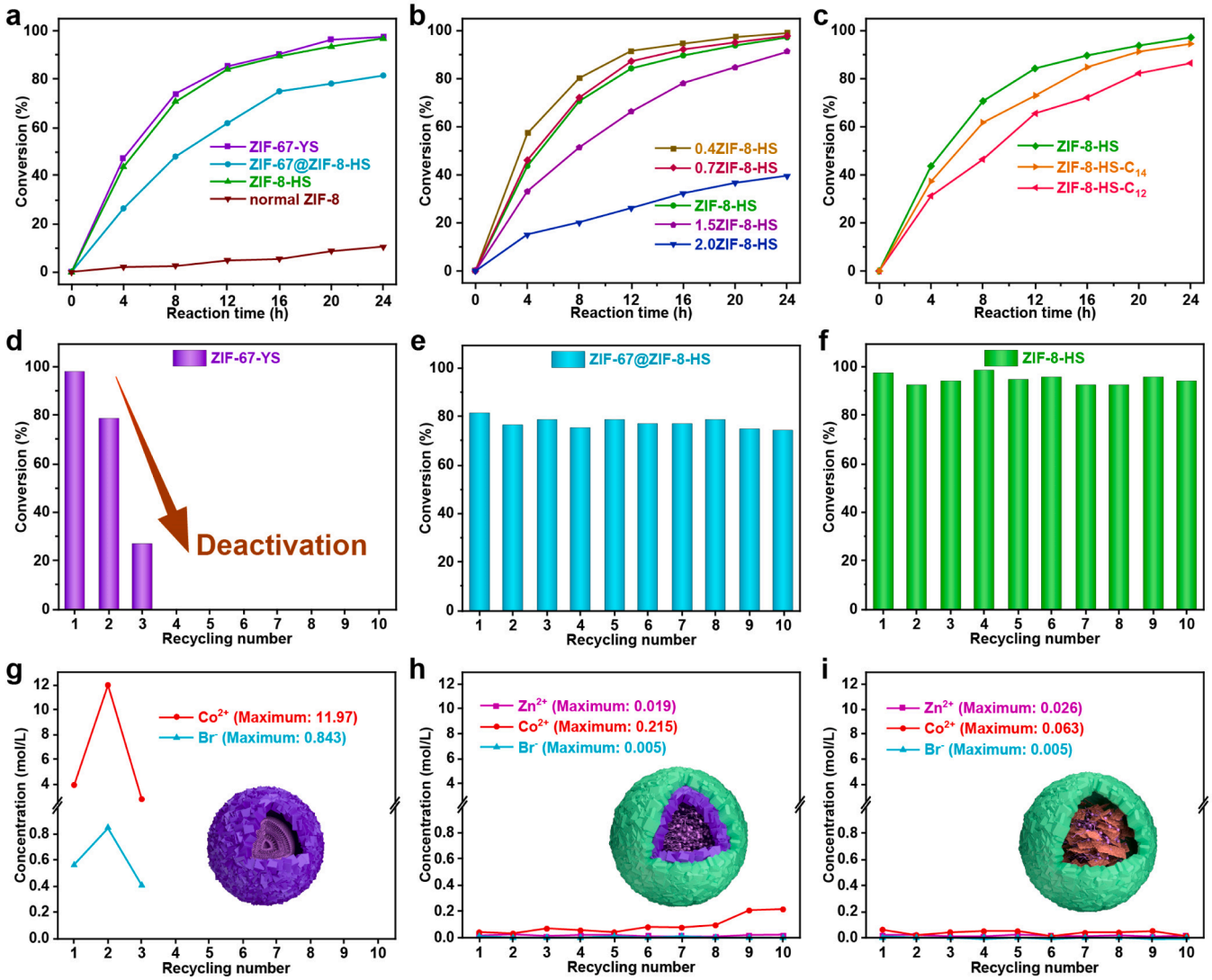

Fig. 4. (a-c) Epichlorohydrin conversions over various catalysts as a function of reaction time. (d-f) Recycling tests of (d) ZIF-67-YS, (e) ZIF-67 @ZIF-8-HS and (f) ZIF-8-HS. (g-i) Concentrations of some representative elements in the reaction liquids after each run for (g) ZIF-67-YS, (h) ZIF-67 @ZIF-8-HS, and (i) ZIF-8-HS.

thickness, the conversion of epichlorohydrin reduces gradually from 90% for 0.4-ZIF-8-HS to 63% for 1.5-ZIF-8-HS after 12 h of reaction time, because thicker shell of m-ZIF-8-HS can certainly lead to higher diffusion resistance of reactants. Not surprisingly, further increasing the shell thickness to about 132 nm, the corresponding 2.0-ZIF-8-HS shows a sharply decreased activity with only 35% conversion of epichlorohydrin after 12 h, because its hollow structure has been partly broken and thus can not well prevent CTAB molecules from leaching.

The catalytic activities of various ZIF-8-HS-C_n were then measured to investigate the influence of alkyl chain length of cocatalysts. As shown in Fig. 4c, with the decrease of alkyl chain length, the conversion of epichlorohydrin (after 24 h of reaction time) is also decreased from 98% for ZIF-8-HS-C_{16} (namely ZIF-8-HS) to 94% for ZIF-8-HS-C_{14}, and finally to 86% for ZIF-8-HS-C_{12}. These results indicate that CTAB with the weakest interaction between $C_{16}TA^+$ and Br^- is the best among all investigated cocatalysts for this reaction [53] Furthermore, to demonstrate the size-selective property of ZIF-8-HS, various epoxides with different functional groups and thus molecule sizes have been employed as substrates [54,55]. Successfully, ZIF-8-HS can afford nearly quantitative conversions for small-size epoxides (epichlorohydrin, epibromohydrin and glycidol) with all above 99% selectivity of their corresponding cyclic carbonate products, indicating its good substrate tolerance to small-size epoxides (Table 1, entries 1–6 and Fig. S18). However, when large-size epoxides such as styrene oxide and cyclohexene oxide are employed as substrates, the catalytic activity of ZIF-8-HS sharply reduces due to their larger molecular sizes (0.49 nm and 0.42 nm, respectively) as compared with the small pore window of ZIF-8 shell (0.34 nm). Specifically, the conversions of styrene oxide and cyclohexene oxide over ZIF-8-HS are only 5% and 3%, respectively, both of which are much lower than those of conventional ZIF-8 with CTAB added as a homogeneous cocatalyst. These results suggest that the continuous ZIF-8 shell of ZIF-8-HS can not only offer CTAB an confined homogeneous environment to prevent its leaching, but also allow the selective penetration of substrates in various sizes and thus endows it with size-selective catalysis for CO_2 fixation.

The greatest merit of heterogeneous catalysts is their good reusability and easy separation from reaction mixtures, which make them much more fascinating in chemical industry as compared with their homogenous counterparts. Thus, to uncover whether our ZIF-8 based nanoreactors can really realize the heterogenization of homogeneous CTAB cocatalyst, we further investigated and compared the recyclability of the ZIF-8-HS, ZIF-67 @ZIF-8-HS and ZIF-67-YS. As shown in Fig. 4d, the epichlorohydrin conversion for ZIF-67-YS decreases drastically from 97% in the first run to 27% in the third run, suggesting the fast deactivation of ZIF-67-YS. In sharp contrast, both of ZIF-67 @ZIF-8-HS and ZIF-8-HS can be reused at least ten times without significant losses of

Table 1
The chemical fixation of CO_2 with various substrates.[a].

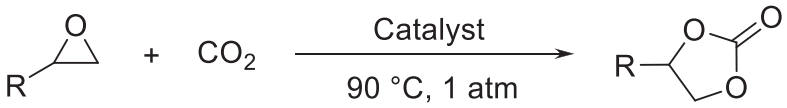

Entry	Catalyst	Epoxides	Products	Con. (%)	Sel. (%)
1	ZIF-8-HS	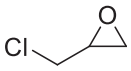	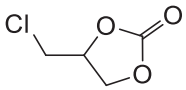	98	99
2	conventional ZIF-8			77	99
3	ZIF-8-HS	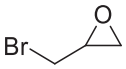	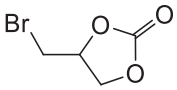	99	99
4	conventional ZIF-8			82	99
5	ZIF-8-HS	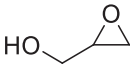	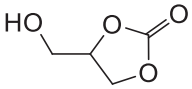	97	98
6	conventional ZIF-8			74	97
7	ZIF-8-HS	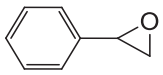	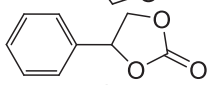	5	97
8	conventional ZIF-8			57	98
9	ZIF-8-HS	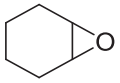	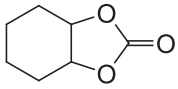	3	98
10	conventional ZIF-8			28	99

[a] Reaction conditions: 5.0 mmol of epoxides, 1 mol% of ZIF-8-HS or conventional ZIF-8 based on Zn content, 0.25 mol% CTAB only added for conventional ZIF-8, 1 atm of CO_2, 90 °C and 24 h. Conversion and yield were measured by GC-MS.

their catalytic activities (Fig. 4e and f), which reveals their much better durability as compared with the ZIF-67 counterpart. Therefore, to further confirm this, we also investigated the potential leaks of Br, Zn and/or Co ions into reaction solutions after each run (the concentrations of Br and Zn/Co ions were measured by IC and AAS, respectively) (Fig. 4g-I, Fig. S19 and Table S3). As expected, nearly undetectable leaks of Br and Zn ions are observed for ZIF-8-HS during the entire recycle test, while there are substantial amounts of Br and Co ions leaching into reaction solutions for ZIF-67-YS after each cycle. Indeed, the SEM, TEM and HAADF-STEM images and the PXRD pattern of the recycled ZIF-67-YS show that the continuous ZIF-67 shell of ZIF-67-YS has been completely destroyed and transformed into thin hollow spheres assembled by cobalt hydroxide nanosheets, which demonstrates the high instability of ZIF-67 under the reaction conditions (Fig. 5a1-a5 and Figs. S20, S21). As a result, most of the CTAB molecules have leaked from the interior cavity of ZIF-67-YS into reaction solution after the recycle tests, as also revealed by the very weak signal of Br in the EDS mapping images of the recycled ZIF-67-YS (Fig. 5). Impressively, the continuous ZIF-8 shell with a hollow structure is well maintained for both of ZIF-8-HS and ZIF-67 @ZIF-8-HS after ten runs, and abundant CTAB molecules are still encapsulated in their interior cavities (Fig. 5b1-b6, c1-c6 and Figs. S22, S23). In addition, it is obvious that the leak of Co ions for ZIF-67 @ZIF-8-HS is much milder than that for ZIF-67-YS after each cycle, which indicates the stable ZIF-8 layer can greatly suppress the structure collapse of ZIF-67 in ZIF-67 @ZIF-8-HS. Based on all above results, we outline the advantages of ZIF-8-HS as compared with its ZIF-67-YS and ZIF-67 @ZIF-8-HS counterparts in Fig. 5d, which can be depicted as follows: (1) though ZIF-67-YS successfully encapsulates abundant Br-based cocatalyst molecules into its cavity, and thus exhibits good synergic catalytic activity in the first run, the high instability restricts its application as a good recyclable catalyst for the chemical fixation of CO_2; (2) after the epitaxial growth of a stable ZIF-8 layer on ZIF-67-YS, the obtained ZIF-67 @ZIF-8-HS shows remarkably improved durability, but the increase of shell thickness can also results in sluggish kinetic process and thus unsatisfactory catalytic efficiency; (3) after the selective etching of the unstable ZIF-67 layer, the resultant ZIF-8-HS displays both fast diffusion rate of reactants and good reusability due to its short diffusion distance and highly stable ZIF-8 shell. Therefore, it is obvious that the rational design of hollow ZIF-8 nanoreactors can be used as a good strategy to heterogenize homogeneous Br-based co-catalysts for the chemical fixation of CO_2 with epoxides.

3.4. Proposed catalytic mechanism

To gain a better understanding of the synergetic catalysis of ZIF-8-HS, we carried out a set of control experiments (Table S2). Clearly, the homogeneous $Zn(NO_3)_2$ exhibits no activity alone but gives 22% conversion of epichlorohydrin in the presence of CTAB, which is more than twice the result when only CTAB is used as a catalyst (Table S2, entries 1, 4 and 5). However, the improvement of catalytic activity is almost negligible for 2-methylimidazole and cobalt hydroxides when they are coupled with CTAB (Table S2, entries 1–3, 6 and 7). These results indicate that the acidic Zn^{2+} ions instead of 2-methylimidazole or cobalt hydroxides can serve as the active centers for this reaction through the synergetic catalysis with CTAB. Furthermore, the physical mixture of ZIF-8 and CTAB gives much lower activity than ZIF-8-HS for the cycloaddition of CO_2 with small-size epichlorohydrin (Fig. 1a and Table 1). The better performance of ZIF-8-HS can be attributed to its continuous but thin MOF shell, which not only possesses abundant highly-exposed Lewis acidic sites with intrinsic catalytic activity, but also offers a confined environment, where CO_2 and epoxides as well as CTAB can be concentrated for boosting the catalytic activity. Therefore, the abundant acidic sites of ZIF-8-HS confirmed by NH_3 temperature-programmed desorption (NH_3-TPD) measurement play an important role in the fixation reaction of CO_2 with epoxides (Fig. S24). Additionally, CO_2-TPD measurement also suggests the presence of basic sites in ZIF-8-HS, which also help to adsorb and aggregate CO_2 molecules around active centers to facilitate the process of reaction (Fig. S25). Moreover, a hot filtration experiment was performed over ZIF-8-HS for the cycloaddition of CO_2 with epichlorohydrin. As shown in Fig. S26, no more increment in the conversion of epichlorohydrin is observed after a filtration process, suggesting the heterogeneous nature of our catalytic system. Thus, based on all above experimental results as well as the previous literature reports [56,57], we propose a catalytic mechanism for the fixation of CO_2 with epoxides over our ZIF-8-HS nanoreactors (Fig. 5e). First, the oxygen end of epoxides is bound on the Lewis acidic zinc sites of ZIF-8 shell to activate the epoxy ring. The nucleophilic attack of Br^- from CTAB then takes place on the less-hindered carbon of

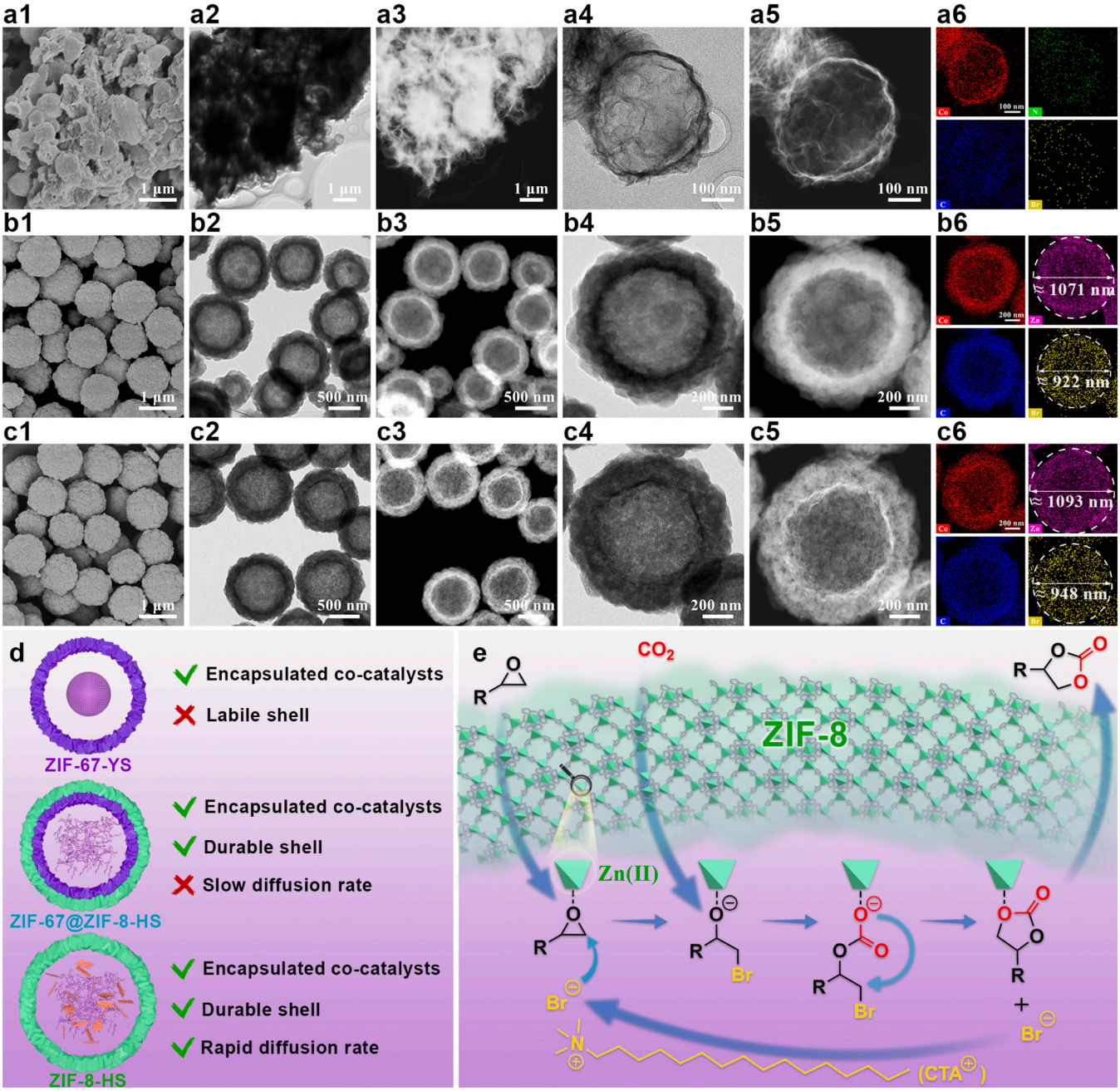

Fig. 5. (a1-c1) SEM, (a2-c2, a4-c4) TEM, (a3-c3, a5-c5) HAADF-STEM and (a6-c6) EDS mapping images of ZIF-67-YS (a1-a6), ZIF-67 @ZIF-8-HS (b1-b6) and ZIF-8-HS (c1-c6) after the recycling tests. (d) Schematic illustration of advantages and disadvantages of ZIF-67-YS, ZIF-67 @ZIF-8-HS and ZIF-8-HS. (e) Proposed catalytic mechanism for the chemical fixation of CO_2 with epoxides over ZIF-8-HS.

activated epoxides and the ring-opened intermediates are obtained, which are stabilized by the zinc sites. This is followed by the addition of a CO_2 molecule with the oxygen anion of ring-opened intermediates to generate the corresponding alkylcarbonate anions, which are then transformed into the cyclic carbonates via an intramolecular ring closing procedure. At last, the cyclic carbonates desorb from the zinc sites and diffuse out of ZIF-8-HS nanoreactors. We infer that such the unique microenvironment of ZIF-8-HS, where the high density of heterogenous Lewis acidic sites and abundant homogenous CTAB molecules as a co-catalyst coexist, can significantly enhance its synergetic catalytic performance for the CO_2 fixation reaction with various epoxides.

4. Conclusions

In summary, we have demonstrated a facile strategy to heterogenize homogeneous Br-based cocatalysts by encapsulating them into hollow ZIF-8 nanoreactors with high stability for the fixation of CO_2 with epoxides. These nanoreactors are prepared in three steps: the synthesis of hollow ZIF-67 spheres by using Br-contained surfactants as soft templates, the controlled growth of a ZIF-8 layer on the above hollow ZIF-67 spheres, and the subsequent etching of the unstable inner ZIF-67 shell. Benefiting from the exploitation of the respective advantages of homogeneous CTAB and heterogeneous ZIF-8 shell as well as the good synergistic effect between them, the resultant ZIF-8-HS shows high catalytic activity, good size-selectivity and excellent recyclability for the CO_2 fixation with epoxides, superior to the traditional catalytic systems, in

which the homogeneous cocatalysts are directly added to the reaction solutions, suffering from complicated product separation/purification process, or immobilized in the nanopore of hosts, resulting in sluggish molecular diffusion and inaccessibility. We believe that this study not only offers a promising heterogeneous catalytic system for carbon fixation, but also sheds light on the heterogenization of other homogeneous catalysts by MOF-based nanoreactors for on-demand synergistic catalysis.

CRediT authorship contribution statement

K.S., Z.Q. and Y.L. conceived the idea and designed the experiments. Z.Q. synthesized the materials, carried out most of the structural characterization and performed the catalytic tests. H.L. X.Y. and L.C. performed some SEM and TEM images. K.S. and Z.Q. cowrote the paper. All authors discussed the results and commented on the manuscript.

Declaration of Competing Interest

The authors declare that they have no known competing financial interests or personal relationships that could have appeared to influence the work reported in this paper.

Acknowledgement

We gratefully acknowledge the financial support from the National Natural Science Foundation of China (22138003, 21825802), Guangdong Natural Science Funds for Distinguished Young Scholar (2018B030306050), and the Natural Science Foundation of Guangdong Province (2017A030312005).

Appendix A. Supporting information

Supplementary data associated with this article can be found in the online version at doi:10.1016/j.apcatb.2022.121163.

References

[1] M. Bui, C.S. Adjiman, A. Bardow, E.J. Anthony, A. Boston, S. Brown, P.S. Fennell, S. Fuss, A. Galindo, L.A. Hackett, J.P. Hallett, H.J. Herzog, G. Jackson, J. Kemper, S. Krevor, G.C. Maitland, M. Matuszewski, I.S. Metcalfe, C. Petit, G. Puxty, J. Reimer, D.M. Reiner, E.S. Rubin, S.A. Scott, N. Shah, B. Smit, J.P.M. Trusler, P. Webley, J. Wilcox, N.M. Dowell, Carbon capture and storage (CCS): the way forward, Energy Environ. Sci. 11 (2018) 1062–1176, https://doi.org/10.1039/C7EE02342A.

[2] Y. He, Q. Lei, C. Li, Y. Han, Z. Shi, S. Feng, Defect engineering of photocatalysts for solar-driven conversion of CO_2 into valuable fuels, Mater. Today 50 (2021) 358–384, https://doi.org/10.1016/j.mattod.2021.03.021.

[3] J. Albero, Y. Peng, H. García, Photocatalytic CO_2 reduction to C2+ products, ACS Catal. 10 (2020) 5734–5749, https://doi.org/10.1021/acscatal.0c00478.

[4] L. Zhang, Z.-J. Zhao, J. Gong, Nanostructured materials for heterogeneous electrocatalytic CO_2 reduction and their related reaction mechanisms, Angew. Chem. Int. Ed. 56 (2017) 11326–11353, https://doi.org/10.1002/anie.201612214.

[5] S. Subramanian, Y. Song, D. Kim, C.T. Yavuz, Redox and nonredox CO_2 utilization: dry reforming of methane and catalytic cyclic carbonate formation, ACS Energy Lett. 5 (2020) 1689–1700, https://doi.org/10.1021/acsenergylett.0c00406.

[6] Q. Liu, L. Wu, R. Jackstell, M. Beller, Using carbon dioxide as a building block in organic synthesis, Nat. Commun. 6 (2015) 5933, https://doi.org/10.1038/ncomms6933.

[7] M. Aresta, A. Dibenedetto, A. Angelini, Catalysis for the valorization of exhaust carbon: from CO_2 to chemicals, materials, and fuels. technological use of CO_2, Chem. Rev. 114 (2014) 1709–1742, https://doi.org/10.1021/cr4002758.

[8] Y.-Y. Zhang, G.-W. Yang, R. Xie, L. Yang, B. Li, G.-P. Wu, Scalable, durable, and recyclable metal-free catalysts for highly efficient conversion of CO_2 to cyclic carbonates, Angew. Chem. Int. Ed. 59 (2020) 23291–23298, https://doi.org/10.1002/anie.202010651.

[9] Y. Xie, T.-T. Wang, X.-H. Liu, K. Zou, W.-Q. Deng, Capture and conversion of CO_2 at ambient conditions by a conjugated microporous polymer, Nat. Commun. 4 (2013) 1960, https://doi.org/10.1038/ncomms2960.

[10] P.-Z. Li, X.-J. Wang, J. Liu, J.S. Lim, R. Zou, Y. Zhao, A triazole-containing metal–organic framework as a highly effective and substrate size-dependent catalyst for CO_2 conversion, J. Am. Chem. Soc. 138 (2016) 2142–2145, https://doi.org/10.1021/jacs.5b13335.

[11] Y. Sun, X. Jia, H. Huang, X. Guo, Z. Qiao, C. Zhong, Solvent-free mechanochemical route for the construction of ionic liquid and mixed-metal MOF composites for synergistic CO_2 fixation, J. Mater. Chem. A 8 (2020) 3180–3185, https://doi.org/10.1039/C9TA10409G.

[12] X. Zhang, H. Liu, Y. Shi, J. Han, Z. Yang, Y. Zhang, C. Long, J. Guo, Y. Zhu, X. Qiu, G. Xue, L. Zhang, B. Zhang, L. Chang, Z. Tang, Boosting CO_2 conversion with terminal alkynes by molecular architecture of graphene oxide-supported Ag nanoparticles, Matter 3 (2020) 558–570, https://doi.org/10.1016/j.matt.2020.07.022.

[13] Z. Guo, C. Xiao, R.V. Maligal-Ganesh, L. Zhou, T.W. Goh, X. Li, D. Tesfagaber, A. Thiel, W. Huang, Pt nanoclusters confined within metal–organic framework cavities for chemoselective cinnamaldehyde hydrogenation, ACS Catal. 4 (2014) 1340–1348, https://doi.org/10.1021/cs400982n.

[14] Z. Qi, Y. Pei, T.W. Goh, Z. Wang, X. Li, M. Lowe, R.V. Maligal-Ganesh, W. Huang, Conversion of confined metal@ZIF-8 structures to intermetallic nanoparticles supported on nitrogen-doped carbon for electrocatalysis, Nano Res. 11 (2018) 3469–3479, https://doi.org/10.1007/s12274-018-2016-x.

[15] C. He, J. Liang, Y.-H. Zou, J.-D. Yi, Y.-B. Huang, R. Cao, Metal-organic frameworks bonded with metal N-heterocyclic carbenes for efficient catalysis, Natl. Sci. Rev. (2021), https://doi.org/10.1093/nsr/nwab157.

[16] L. Zeng, Z. Wang, Y. Wang, J. Wang, Y. Guo, H. Hu, X. He, C. Wang, W. Lin, Photoactivation of Cu centers in metal–organic frameworks for selective CO_2 conversion to ethanol, J. Am. Chem. Soc. 142 (2020) 75–79, https://doi.org/10.1021/jacs.9b11443.

[17] B. An, L. Zeng, M. Jia, Z. Li, Z. Lin, Y. Song, Y. Zhou, J. Cheng, C. Wang, W. Lin, Molecular iridium complexes in metal–organic frameworks catalyze CO_2 hydrogenation via concerted proton and hydride transfer, J. Am. Chem. Soc. 139 (2017) 17747–17750, https://doi.org/10.1021/jacs.7b10922.

[18] A. Primo, J. He, B. Jurca, B. Cojocaru, C. Bucur, V.I. Parvulescu, H. Garcia, CO_2 methanation catalyzed by oriented MoS_2 nanoplatelets supported on few layers graphene, Appl. Catal. B Environ. 245 (2019) 351–359, https://doi.org/10.1016/j.apcatb.2018.12.034.

[19] D. Liu, G. Li, H. Guo, J. Liu, Facile preparation of bi-functional iron doped mesoporous materials and their application in the cycloaddition of CO_2, J. Energy Chem. 41 (2020) 52–59, https://doi.org/10.1016/j.jechem.2019.05.005.

[20] D. Liu, G. Li, J. Liu, Y. Wei, H. Guo, Mesoporous titanium-silicalite zeolite containing organic templates as a bifunctional catalyst for cycloaddition of CO_2 and epoxides, ACS Appl. Mater. Interfaces 10 (2018) 22119–22129, https://doi.org/10.1021/acsami.8b04759.

[21] Y.-X. Liu, H.-H. Wang, T.-J. Zhao, B. Zhang, H. Su, Z.-H. Xue, X.-H. Li, J.-S. Chen, Schottky barrier induced coupled interface of electron-rich N-doped carbon and electron-deficient Cu: in-built Lewis acid–base pairs for highly efficient CO_2 fixation, J. Am. Chem. Soc. 141 (2019) 38–41, https://doi.org/10.1021/jacs.8b08267.

[22] M. Ciprian, K.H. Ruiz, M. Kassymova, T. Wang, S. Zhuiykov, S. Chaemchuen, R. Tu, F. Verpoort, 3D derived N-doped carbon matrix from 2D ZIF-L as an enhanced stable catalyst for chemical fixation, Micro Mesoporous Mater. 285 (2019) 80–88, https://doi.org/10.1016/j.micromeso.2019.04.053.

[23] Z. Dai, Q. Sun, X. Liu, C. Bian, Q. Wu, S. Pan, L. Wang, X. Meng, F. Deng, F.-S. Xiao, Metalated porous porphyrin polymers as efficient heterogeneous catalysts for cycloaddition of epoxides with CO_2 under ambient conditions, J. Catal. 338 (2016) 202–209, https://doi.org/10.1016/j.jcat.2016.03.005.

[24] A. Giri, N.N. Patil, A. Patra, Porous noria polymer: a cage-to-network approach toward a robust catalyst for CO_2 fixation and nitroarene reduction, Chem. Commun. 57 (2021) 4404–4407, https://doi.org/10.1039/D0CC07805K.

[25] G. Zhai, Y. Liu, Y. Mao, H. Zhang, L. Lin, Y. Li, Z. Wang, H. Cheng, P. Wang, Z. Zheng, Y. Dai, B. Huang, Improved photocatalytic CO_2 and epoxides cycloaddition via the synergistic effect of Lewis acidity and charge separation over Zn modified UiO-bpydc, Appl. Catal. B Environ. 301 (2022), 120793, https://doi.org/10.1016/j.apcatb.2021.120793.

[26] Z. Fang, Z. Deng, X. Wan, Z. Li, X. Ma, S. Hussain, Z. Ye, X. Peng, Keggin-type polyoxometalates molecularly loaded in Zr-ferrocene metal organic framework nanosheets for solar-driven CO_2 cycloaddition, Appl. Catal. B Environ. 296 (2021), 120329, https://doi.org/10.1016/j.apcatb.2021.120329.

[27] X. Zhang, H. Liu, P. An, Y. Shi, J. Han, Z. Yang, C. Long, J. Guo, S. Zhao, K. Zhao, H. Yin, L. Zheng, B. Zhang, X. Liu, L. Zhang, G. Li, Z. Tang, Delocalized electron effect on single metal sites in ultrathin conjugated microporous polymer nanosheets for boosting CO_2 cycloaddition, Sci. Adv. 6 (2020) eaaz4824, https://www.science.org/doi/abs/10.1126/sciadv.aaz4824.

[28] S. Zhang, Q. Wang, P. Puthiaraj, W.-S. Ahn, MgFeAl layered double hydroxide prepared from recycled industrial solid wastes for CO_2 fixation by cycloaddition to epoxides, J. CO2 Util. 34 (2019) 395–403, https://doi.org/10.1016/j.jcou.2019.07.035.

[29] R. Cao, Y.-H. Zou, Y.-B. Huang, D.-H. Si, Q. Yin, Q.-J. Wu, Z. Weng, Porous metal–organic framework liquids for enhanced CO_2 adsorption and catalytic conversion, Angew. Chem. Int. Ed. 60 (2021) 20915–20920, https://doi.org/10.1002/anie.202107156.

[30] N. Wei, Y. Zhang, L. Liu, Z.-B. Han, D.-Q. Yuan, Pentanuclear Yb(III) cluster-based metal-organic frameworks as heterogeneous catalysts for CO_2 conversion, Appl. Catal. B: Environ. 219 (2017) 603–610, https://doi.org/10.1016/j.apcatb.2017.07.085.

[31] D. Ma, B. Li, K. Liu, X. Zhang, W. Zou, Y. Yang, G. Li, Z. Shi, S. Feng, Bifunctional MOF heterogeneous catalysts based on the synergy of dual functional sites for efficient conversion of CO_2 under mild and co-catalyst free conditions, J. Mater. Chem. A 3 (2015) 23136–23142, https://doi.org/10.1039/C5TA07026K.

[32] B. Aguila, Q. Sun, X. Wang, E. O'Rourke, A.M. Al-Enizi, A. Nafady, S. Ma, Lower activation energy for catalytic reactions through host–guest cooperation within metal–organic frameworks, Angew. Chem. Int. Ed. 57 (2018) 10107–10111, https://doi.org/10.1002/anie.201803081.
[33] H. He, Q. Zhu, C. Zhang, Y. Yan, J. Yuan, J. Chen, C. Li, M. Du, Encapsulation of an ionic metalloporphyrin into a zeolite imidazolate framework in situ for CO_2 chemical transformation via host–guest synergistic catalysis, Chem. Asian J. 14 (2019) 958–962, https://doi.org/10.1002/asia.201900021.
[34] W. Xiong, H. Li, H. You, M. Cao, R. Cao, Encapsulating metal organic framework into hollow mesoporous carbon sphere as efficient oxygen bifunctional electrocatalyst, Natl. Sci. Rev. 7 (2020) 609–619, https://doi.org/10.1093/nsr/nwz166.
[35] Y. Guo, W. Shi, H. Yang, Q. He, Z. Zeng, J. Ye, X. He, R. Huang, C. Wang, W. Lin, Cooperative stabilization of the [Pyridinium- CO_2-Co] adduct on a metal–organic layer enhances electrocatalytic CO_2 reduction, J. Am. Chem. Soc. 141 (2019) 17875–17883, https://doi.org/10.1021/jacs.9b09227.
[36] X. Hu, P. Chen, C. Zhang, Z. Wang, C. Wang, Energy transfer on a two-dimensional antenna enhances the photocatalytic activity of CO_2 reduction by metal–organic layers, Chem. Commun. 55 (2019) 9657–9660, https://doi.org/10.1039/C9CC04594E.
[37] X.-Y. Liu, F. Zhang, T.-W. Goh, Y. Li, Y.-C. Shao, L. Luo, W. Huang, Y.-T. Long, L.-Y. Chou, C.-K. Tsung, Using a multi-shelled hollow metal–organic framework as a host to switch the guest-to-host and guest-to-guest interactions, Angew. Chem. Int. Ed. 57 (2018) 2110–2114, https://doi.org/10.1002/anie.201711600.
[38] Y. Pei, Z. Qi, X. Li, R.V. Maligal-Ganesh, T.W. Goh, C. Xiao, T. Wang, W. Huang, Morphology inherence from hollow MOFs to hollow carbon polyhedrons in preparing carbon-based electrocatalysts, J. Mater. Chem. A 5 (2017) 6186–6192, https://doi.org/10.1039/C6TA10609A.
[39] C. Zhang, Y.-C. Wang, B. An, R. Huang, C. Wang, Z. Zhou, W. Lin, Networking pyrolyzed zeolitic imidazolate frameworks by carbon nanotubes improves conductivity and enhances oxygen-reduction performance in polymer-electrolyte-membrane fuel cells, Adv. Mater. 29 (2017), 1604556, https://doi.org/10.1002/adma.201604556.
[40] Y. Guo, H. Yang, X. Zhou, K. Liu, C. Zhang, Z. Zhou, C. Wang, W. Lin, Electrocatalytic reduction of CO_2 to CO with 100% faradaic efficiency by using pyrolyzed zeolitic imidazolate frameworks supported on carbon nanotube networks, J. Mater. Chem. A 5 (2017) 24867–24873, https://doi.org/10.1039/C7TA08431E.
[41] X. Lan, N. Huang, J. Wang, T. Wang, A general and facile strategy for precisely controlling the crystal size of monodispersed metal–organic frameworks via separating the nucleation and growth, Chem. Commun. 54 (2018) 584–587, https://doi.org/10.1039/C7CC08244D.
[42] X. Lan, N. Huang, J. Wang, T. Wang, Geometric effect in the highly selective hydrogenation of 3-methylcrotonaldehyde over Pt@ZIF-8 core–shell catalysts, Catal. Sci. Technol. 7 (2017) 2601–2608, https://doi.org/10.1039/C7CY00353F.
[43] X. Lan, B. Ali, Y. Wang, T. Wang, Hollow and yolk–shell Co-N-C@SiO_2 nanoreactors: controllable synthesis with high selectivity and activity for nitroarene hydrogenation, ACS Appl. Mater. Interfaces 12 (2020) 3624–3630, https://doi.org/10.1021/acsami.9b19364.
[44] X. Gao, M. Liu, J. Lan, L. Liang, X. Zhang, J. Sun, Lewis acid–base bifunctional crystals with a three-dimensional framework for selective coupling of CO_2 and epoxides under mild and solvent-free conditions, Cryst. Growth Des. 17 (2017) 51–57, https://doi.org/10.1021/acs.cgd.6b01132.
[45] M. Zhu, D. Srinivas, S. Bhogeswararao, P. Ratnasamy, M.A. Carreon, Catalytic activity of ZIF-8 in the synthesis of styrene carbonate from CO_2 and styrene oxide, Catal. Commun. 32 (2013) 36–40, https://doi.org/10.1016/j.catcom.2012.12.003.
[46] F. Yang, H. Mu, C. Wang, L. Xiang, K.X. Yao, L. Liu, Y. Yang, Y. Han, Y. Li, Y. Pan, Morphological map of ZIF-8 crystals with five distinctive shapes: feature of filler in mixed-matrix membranes on C_3H_6/C_3H_8 separation, Chem. Mater. 30 (2018) 3467–3473, https://doi.org/10.1021/acs.chemmater.8b01073.
[47] J. Tang, R.R. Salunkhe, J. Liu, N.L. Torad, M. Imura, S. Furukawa, Y. Yamauchi, Thermal conversion of core–shell metal–organic frameworks: a new method for selectively functionalized nanoporous hybrid carbon, J. Am. Chem. Soc. 137 (2015) 1572–1580, https://doi.org/10.1021/ja511539a.
[48] Y.C. Tan, H.C. Zeng, Self-templating synthesis of hollow spheres of MOFs and their derived nanostructures, Chem. Commun. 52 (2016) 11591–11594, https://doi.org/10.1039/C6CC05699G.
[49] B. Sun, H.C. Zeng, A shell-by-shell approach for synthesis of mesoporous multi-shelled hollow MOFs for catalytic applications, Part. Part. Syst. Charact. 37 (2020), 2000101, https://doi.org/10.1002/ppsc.202000101.
[50] M. Bielawska, A. Chodzińska, B. Jańczuk, A. Zdziennicka, Determination of CTAB CMC in mixed water + short-chain alcohol solvent by surface tension, conductivity, density and viscosity measurements, Colloids Surf. A: Physicochem. Eng. Asp. 424 (2013) 81–88, https://doi.org/10.1016/j.colsurfa.2013.02.017.
[51] G. Zhan, H.C. Zeng, ZIF-67–derived nanoreactors for controlling product selectivity in CO_2 hydrogenation, ACS Catal. 7 (2017) 7509–7519, https://doi.org/10.1021/acscatal.7b01827.
[52] H. Chen, K. Shen, Q. Mao, J. Chen, Y. Li, Nanoreactor of MOF–derived yolk–shell Co@C–N: precisely controllable structure and enhanced catalytic activity, ACS Catal. 8 (2018) 1417–1426, https://doi.org/10.1021/acscatal.7b03270.
[53] C. Carvalho Rocha, T. Onfroy, J. Pilmé, A. Denicourt-Nowicki, A. Roucoux, F. Launay, Experimental and theoretical evidences of the influence of hydrogen bonding on the catalytic activity of a series of 2-hydroxy substituted quaternary ammonium salts in the styrene oxide/CO_2 coupling reaction, J. Catal. 333 (2016) 29–39, https://doi.org/10.1016/j.jcat.2015.10.014.
[54] E. López-Maya, N.M. Padial, J. Castells-Gil, C.R. Ganivet, A. Rubio-Gaspar, F. G. Cirujano, N. Almora-Barrios, S. Tatay, S. Navalón, C. Martí-Gastaldo, Selective implantation of diamines for cooperative catalysis in isoreticular heterometallic titanium–organic frameworks, Angew. Chem. Int. Ed. 60 (2021) 11868–11873, https://doi.org/10.1002/anie.202100176.
[55] C.-H. Kuo, Y. Tang, L.-Y. Chou, B.T. Sneed, C.N. Brodsky, Z. Zhao, C.-K. Tsung, Yolk–shell nanocrystal@ZIF-8 nanostructures for gas-phase heterogeneous catalysis with selectivity control, J. Am. Chem. Soc. 134 (2012) 14345–14348, https://doi.org/10.1021/ja306869j.
[56] W.-Y. Gao, Y. Chen, Y. Niu, K. Williams, L. Cash, P.J. Perez, L. Wojtas, J. Cai, Y.-S. Chen, S. Ma, Crystal engineering of an nbo topology metal–organic framework for chemical fixation of CO_2 under ambient conditions, Angew. Chem. Int. Ed. 53 (2014) 2615–2619, https://doi.org/10.1002/anie.201309778.
[57] W. Xiang, Z. Sun, Y. Wu, L.-N. He, C. Liu, Enhanced cycloaddition of CO_2 to epichlorohydrin over zeolitic imidazolate frameworks with mixed linkers under solventless and co-catalyst-free condition, Catal. Today 339 (2020) 337–343, https://doi.org/10.1016/j.cattod.2019.01.050.